ELSEVIER

J. Non-Newtonian Fluid Mech. 141 (2007) 85–98

Journal of Non-Newtonian Fluid Mechanics

www.elsevier.com/locate/jnnfm

Fully-developed pipe and planar flows of multimode viscoelastic fluids

D.O.A. Cruz [a], F.T. Pinho [b,c,*]

[a] *Departamento de Engenharia Mecânica, Universidade Federal do Pará- UFPa, Campus Universitário do Guamá, 66075-900 Belém, Pará, Brazil*
[b] *Centro de Estudos de Fenómenos de Transporte, Faculdade de Engenharia da, Universidade do Porto, 4200-465 Porto, Portugal*
[c] *Universidade do Minho, Largo do Paço, 4704-553 Braga, Portugal*

Received 2 May 2006; received in revised form 19 July 2006; accepted 1 September 2006

Abstract

Two solutions are presented for fully-developed pipe and planar flows of multimode viscoelastic models. The fluids have a Newtonian solvent contribution and the polymer modes are described by the Phan-Thien—Tanner (PTT), the FENE-P or the Giesekus equation. The first solution is exact and can handle any number of modes, but is only semi-analytical. The second solution, which is presented only for the PTT model with a linear stress coefficient and the FENE-P model, can also handle any number of modes. It is based on a truncated series expansion and is completely analytical, but provides only an approximated solution. The complexity of the multimode solutions is investigated first with the exact semi-analytical method and it is shown that at high Deborah number flows the high-order stresses can become as important as the stress of the first mode. It is also under these conditions that the approximated analytical solution deviates from the exact semi-analytical solution. A criterion for the accurate use of the approximated solution is presented. Fortran codes are provided to obtain these solutions at the internet address at the end.

Keywords: Multimode viscoelastic models; PTT; FENE-P; Giesekus; Pipe flow; Planar flow

1. Introduction

Nonlinear differential constitutive equations are increasingly used to describe the rheology of viscoelastic fluids and in solving fluid mechanics problems of relevance to polymer melts and solutions. Analytical solutions of such problems provide strong insight and are also useful for validation and verification purposes. However, analytical solutions can only be obtained for simple constitutive models and/or under simplifying flow conditions, such as flow symmetry and fully-developed flow conditions, which lead to integrable expressions. As a consequence, most of the studies in the literature concern single-mode models. A few examples for viscoelastic constitutive equations are: Beris et al. [1] for concentric and eccentric annular flow of Maxwell, White–Metzner and Criminale–Eriksen–Filbey (CEF) fluid models, Cruz and Pinho [2] for skewed Poiseuille-Couette flows of Phan-Thien—Tanner (PTT) fluids, Oliveira [3] for pipe and planar flows of a FENE-P fluid (Finitely-Extensible-Nonlinear-Elastic dumbbell model with Peterlin approximation), for Giesekus fluids, the works of Schleiniger and Weinacht [4] for pipe and planar flows and of Yoo and Choi [5] for Couette and planar flows. Van Schaftingen and Crochet [6] have developed an analytical solution for the Poiseuille flow of Johnson–Segalman fluid model. The various works of Oliveira, Pinho and co-workers [7–9] and of Hashemabadi et al. [10,11] are for isothermal and non-isothermal pipe and planar flows of PTT and FENE-P fluids.

Whereas these works were aimed at investigating the characteristics of steady flow conditions, other analytical contributions investigated stability issues. It is the case of Hulsen [12] and Siline and Leonov [13] for the Giesekus and Leonov models, but also of Georgiou [14] for the Oldroyd-B model and of Georgiou and Vlassopoulos [15] for the model of Johnson and Segalman [16] in steady flow and of Fyrillas et al. [17] for unsteady flows. Many other analytical contributions can be found in the specialized journals, such as the Journal of Non-Newtonian Fluid Mechanics and Rheologica Acta, or earlier in the Quaterly Journal of Mechanics and Applied Mathematics, among others.

However, the complex rheology of viscoelastic polymer melts and polymer solutions usually requires the use of multimode models for an adequate description of the fluid behaviour. The coupling between the various modes and the flow kinematics

* Corresponding author at: Centro de Estudos de Fenómenos de Transporte, Faculdade de Engenharia da Universidade do Porto, Rua Dr. Roberto Frias s/n, 4200-465 Porto, Portugal. Tel.: +351 967 170 674; fax: +351 225082153/1445.
E-mail addresses: doac@ufpa.br (D.O.A. Cruz), fpinho@fe.up.pt (F.T. Pinho).

0377-0257/$ – see front matter © 2006 Elsevier B.V. All rights reserved.
doi:10.1016/j.jnnfm.2006.09.001

makes analytical solutions for multimode models a rather challenging task, so the tendency is to use computational rheology tools to obtain numerical solutions [18–20]. Needless to say that in most cases there is no other choice, but for very simple geometries a semi-analytical solution is possible.

In this paper we present two alternative solutions for fully-developed pipe and planar flow of multimode models based on the PTT and the FENE-P equations, with one of the solutions also presented for the Giesekus model. The first solution is exact, but is semi-analytical and depends on the corresponding analytical solution for the single-mode model, an indication that the methodology described can be extended to other fluids or flows provided the corresponding single mode analytical solution exists. The second solution is fully analytical, but invokes simplifying assumptions and consequently it is only approximate. This being a perturbed solution, it should be possible to produce also an approximate solution for the multimode Giesekus model, but this is not attempted here given its limited scope and higher degree of complexity.

In Section 2 we present the governing equations necessary to solve the pipe and planar flow problems for the multimode linear and exponential PTT models. Section 3 describes the method to obtain the corresponding exact semi-analytical solutions. This is followed by the presentation and discussion of some results showing the application of the method to illustrate some differences between the flow of fluids modeled by a multimode model and the corresponding single-mode model. In Section 4, the alternative approximate fully analytical solution is derived for the linear form of the PTT model after formulating some simplifying assumptions and this is followed by a comparison of its results with those from the exact method and the definition of a criterion for the applicability of the approximate solution. Section 5 presents the approximate solutions for the planar flow of the linear PTT model, the transformations required to obtain the exact and approximate pipe and planar flow solutions for a multimode FENE-P fluid and the equations necessary to obtain the semi-analytical exact solution for a multimode Giesekus model.

2. Governing equations

For fully-developed pipe or planar flows the momentum equation in the streamwise z-direction simplifies to

$$\frac{1}{y}\frac{\mathrm{d}}{\mathrm{d}r}(y\tau_{rz,F}) - \frac{\mathrm{d}p}{\mathrm{d}z} = 0 \tag{1}$$

where r designates the radial coordinate in pipe flow or the transverse coordinate in planar flow, p is the pressure and τ_{rz} is the rz stress component. For pipe flow $y = r$ whereas for planar flow $y = 1$. Subscript F is used to denote the extra fluid stress, which for a multimode model has N individual polymer contributions ($\tau_{ij,m}$) and one solvent ($\tau_{ij,s}$) contribution, as given by Eq. (2).

$$\tau_{ij,F} = \sum_{m=1}^{N} \tau_{ij,m} + \tau_{ij,s}. \tag{2}$$

The fluid dynamic solution is unique and is characterized by a streamwise velocity profile (u), the radial and tangential velocities being null.

Each polymer mode $\tau_{ij,m}$ obeys the PTT constitutive equation derived by Phan-Thien and Tanner [21]. Here, the simplified version of the model with a zero second normal stress difference is being considered ($\xi = 0$), which is given by Eq. (3) for each mode m.

$$f(\tau_{kk,m})\tau_{ij,m} + \lambda_m \overset{\nabla}{\tau}_{ij,m} = 2\eta_m D_{ij} \tag{3}$$

The stress coefficient function $f(\tau_{kk})$ takes either the exponential form (Eq. (4)) or its linearised form (Eq. (5)),

$$f(\tau_{kk,m}) = \exp\left(\frac{\lambda_m \varepsilon_m}{\eta_m}\tau_{kk,m}\right) \tag{4}$$

$$f(\tau_{kk,m}) = 1 + \frac{\lambda_m \varepsilon_m}{\eta_m}\tau_{kk,m} \tag{5}$$

For each polymer mode λ_m, η_m and ε_m are the relaxation time, the polymer viscosity coefficient and a parameter limiting the extensional viscosity, respectively. D_{ij} is the rate of deformation tensor defined in (Eq. (6)) and $\overset{\nabla}{\tau}_{ij,m}$ represents Oldroyd's upper convected derivative defined in Eq. (7).

$$D_{ij} = \frac{(\nabla u)_{ij} + (\nabla u)_{ij}^{T}}{2} \tag{6}$$

$$\overset{\nabla}{\tau}_{ij} = \frac{\partial \tau_{ij}}{\partial t} + u_k \frac{\partial \tau_{ij}}{\partial x_k} - \tau_{ik}\frac{\partial u_j}{\partial x_k} - \tau_{kj}\frac{\partial u_i}{\partial x_k}. \tag{7}$$

The Newtonian solvent contribution appearing in Eq. (2) is given by

$$\tau_{ij,s} = 2\eta_s D_{ij} \tag{8}$$

where η_s is the solvent viscosity.

3. Exact semi-analytical solution

For fully-developed pipe and planar flows the constitutive equation for each polymer mode simplifies to the following set, with Eq. (9c) accounting for the solvent contribution to the shear stress.

$$\tau_{rz,m} = \frac{\eta_m}{f(\tau_{kk,m})}\frac{\partial u}{\partial r} \tag{9a}$$

$$\tau_{zz,m} = \frac{2\lambda_m \eta_m}{f(\tau_{kk,m})^2}\left(\frac{\partial u}{\partial r}\right)^2 \tag{9b}$$

$$\tau_{rz,S} = \eta_s \frac{\partial u}{\partial r} \tag{9c}$$

Eqs. (9a) and (9b) are identical to those for a single mode model with the same stress function $f(\tau_{kk,m})$. The shear rate of the flow is mode-independent and couples all modes through the momentum balance. As for the single mode model [7], the other four components of the polymer stress tensor

($\tau_{\theta\theta} = \tau_{rr} = \tau_{r\theta} = \tau_{\theta z}$) are null and the two non-zero stresses are related via Eq. (10).

$$\tau_{rz,m} = \sqrt{\frac{\eta_m \tau_{zz,m}}{2\lambda_m}} \tag{10}$$

As for a single mode fluid [7], the solution of the above equations for the multimode fluid involves the coupling between the normal and shear stresses. By back-substitution it is possible to relate the axial velocity with the normal stress for a given streamwise pressure gradient. Although conceptually the procedure is identical to that for a single mode model the solution for the multimode model is more involving and requires a numerical solution.

Henceforth, we will rewrite any modal normal stress as a function of a single normal stress, which we will refer to as the principal stress $\tau_{zz,p}$ (subscript p). For convenience, the principal mode will always be the first mode ($\tau_{zz,1}$). Eq. (9b) is used to relate the principal normal stress with any modal normal stress, defining function ϕ_p, which is written in the form of Eq. (11).

$$\phi_p = \frac{\tau_{zz,p} f_p^2}{\lambda_p \eta_p} = \frac{\tau_{zz,m} f_m^2}{\lambda_m \eta_m} \tag{11}$$

For compactness, we write $f_p \equiv f(\tau_{zz,p})$ and $f_m = f(\tau_{zz,m})$.

In Sections 3.1 and 3.2, Eq. (11) is used to obtain $\tau_{zz,m}$ as a function of ϕ_p for the linear and exponential PTT models, respectively. Then, the momentum Eq. (1) is used together with Eqs. (9b) and (10) to arrive at explicit expressions for the principal normal stress and the velocity gradient, but their integration to determine $\tau_{zz,p}$ and u must be carried out numerically.

3.1. Linear PTT model

For the linear PTT model, Eq. (11) is a cubic equation to determine $\tau_{zz,m}$ written as

$$\tau_{zz,m}^3 + a_1 \tau_{zz,m}^2 + a_2 \tau_{zz,m} + a_3 = 0 \tag{12}$$

with coefficients

$$a_1 = \frac{2\eta_m}{\varepsilon_m \lambda_m} \tag{13a}$$

$$a_2 = \frac{\eta_m^2}{\varepsilon_m^2 \lambda_m^2} \tag{13b}$$

$$a_3 = -\frac{\eta_m^3}{\varepsilon_m^2 \lambda_m} \phi_p \tag{13c}$$

The real solution of this cubic equation is available in the specialized literature and is given by

$$\tau_{zz,m} = \sqrt[3]{R_m + \sqrt{Q_m^3 + R_m^2}} + \sqrt[3]{R_m - \sqrt{Q_m^3 + R_m^2}} - \frac{1}{3} a_1 \tag{14}$$

with

$$R_m = \frac{9a_1 a_2 - 27a_3 - 2a_1^3}{54} = \frac{1}{2} \frac{\eta_m^3}{\lambda_m \varepsilon_m^2} \phi_p + \frac{1}{27} \frac{\eta_m^3}{\lambda_m^3 \varepsilon_m^3} \tag{15a}$$

$$Q_m = \frac{3a_2 - a_1^2}{9} = -\frac{1}{9} \frac{\eta_m^2}{\lambda_m^2 \varepsilon_m^2} \tag{15b}$$

Using Eqs. (10) and (11) and the linear radial variation of $\tau_{ij,F}$ (from integration of the momentum equation), the following equation for $\tau_{zz,P}$ is obtained:

$$\frac{\mathrm{d}p}{\mathrm{d}z} \frac{r}{2^q} = \sqrt{\frac{\eta_p \tau_{zz,p}}{2\lambda_p}} + \sum_{m=2}^{N} \sqrt{\frac{\eta_m}{2\lambda_m} \tau_{zz,m}} + \eta_s \frac{\mathrm{d}u}{\mathrm{d}r} \tag{16}$$

where the velocity gradient is calculated with Eq. (9b) using the principal normal stress

$$\frac{\mathrm{d}u}{\mathrm{d}r} = \sqrt{\frac{\tau_{zz,p}}{2\lambda_p \eta_p}} \left(1 + \frac{\varepsilon_p \lambda_p}{\eta_p} \tau_{zz,p}\right) \tag{17}$$

Eq. (16) is valid for both pipe ($q = 1$) and planar ($q = 0$) flows. Its solution is numerical and provides the relationship between $\tau_{zz,P}$ and the pipe radius (or cross-stream coordinate for the flow between two parallel plates), whereas the velocity profile is given by numerical integration of Eq. (17). The need for numerical solutions stem from the dependence of $\tau_{zz,m}$ on $\tau_{zz,P}$ via ϕ_p.

3.2. Exponential PTT model

For the exponential PTT model an iterative process is required to calculate $\tau_{zz,m}$ since an explicit expression for this quantity cannot be obtained as for the linear model. From Eq. (11)

$$\phi_p = \frac{\tau_{zz,p}}{\lambda_p \eta_p} \exp\left(\frac{\varepsilon_p \lambda_p}{\eta_p} 2\tau_{zz,p}\right) = \frac{\tau_{zz,m}}{\lambda_m \eta_m} \exp\left(\frac{\varepsilon_m \lambda_m}{\eta_m} 2\tau_{zz,m}\right) \tag{18}$$

and rewriting this equation in order to $\tau_{zz,m}$ gives

$$\tau_{zz,m}^{(n)} = \tau_{zz,p} \frac{\lambda_m \eta_m}{\lambda_p \eta_p} \exp\left(2\frac{\varepsilon_p \lambda_p}{\eta_p} \tau_{zz,p} - 2\frac{\varepsilon_m \lambda_m}{\eta_m} \tau_{zz,m}^{(n-1)}\right) \tag{19}$$

where superscripts (n) and $(n-1)$ designate the level of iteration. As a first guess for $\tau_{zz,m}$, the solution for the linear PTT model (Eq. (14)) can be used.

Henceforth, the calculation procedure for this model is identical to that for the linear PTT model, i.e., Eq. (16) gives the principal normal stress as a function of pipe radius (transverse coordinate for the planar flow), with the adequate modifications of the stress coefficient function, and the numerical integration of Eq. (20) provides the velocity profile for a given pressure gradient.

$$\frac{\mathrm{d}u}{\mathrm{d}r} = \sqrt{\frac{\tau_{zz,p}}{2\lambda_p \eta_p}} \exp\left(\frac{\varepsilon_p \lambda_p}{\eta_p} \tau_{zz,p}\right) \tag{20}$$

3.3. Results and discussion

To test the above procedure we present and discuss results for the pipe flow of a fluid modeled by four mode PTT equation with a Newtonian solvent contribution. The fluid chosen was based on the multimode PTT model fitted by Alves et al. [22] to the

Table 1
Linear viscoelastic spectrum for PAA500 with $\xi = 0$, from Alves et al. [23]. Fluid 1 has $\eta_s = 0$ and Fluid 3 has $\eta_s = 0.27$ Pa s

Mode	λ_k (s)	η_k (Pa s)
1	30	2.5
2	3	0.9
3	0.3	0.3
4	0.03	0.1
Solvent	–	0.27

rheology of the PAA500 solution (500 ppm by weight of polyacrilamide in a 85% glycerin-15% water mixture) characterized previously by Alves et al. [23]. The four mode linear PTT model of Alves et al. [22], which had constant $\varepsilon = 0.02$, $\xi = 0.04$, a Newtonian solvent contribution and parameters η_k and λ_k listed in Table 1, predicts well the linear viscoelastic spectrum, the steady shear viscosity and the first normal stress difference coefficient of the PAA500 fluid. For the tests in this paper we used a modified multimode model, termed Fluid 1, where parameter $\xi = 0$ (simplified PTT model) and the Newtonian solvent contribution is also removed ($\eta_s = 0$) in order to emphasize the role of the four polymer modes. Of course, the exact solution in Sections 3.1 and 3.2 are more general since they include the Newtonian solvent contribution.

The pipe flow solution of Fluid 1 is compared with that of the corresponding single mode PTT fluid, here called Fluid 2, and for which there is an analytical solution [7]. To obtain parameters η and λ of Fluid 2, from those of the multimode Fluid 1, the following equations are used [24]

$$\eta = \eta_{\text{solvent}} + \eta_p = \eta_{\text{solvent}} + \sum_{k \neq \text{solvent}} \eta_k \tag{21}$$

$$\lambda = \frac{\sum_{k \neq \text{solvent}} \lambda_k \eta_k}{\sum_{k \neq \text{solvent}} \eta_k} \tag{22}$$

which gave $\lambda = 20.48$ s and $\eta = 3.8$ Pa s (for Fluid 2 $\eta_s = 0$ also). These two parameters are based on the Oldroyd-B model and guarantee that at low deformation rates and low angular velocities the viscoelastic behaviour of the single mode PTT (or Oldroyd-B model) is identical to that of the multimode model (say, $\Psi_{1,0} \equiv \lim_{\dot{\gamma} \to 0} \Psi_1 = \sum_k 2\eta_k \lambda_k = 2\eta_p \lambda$).

We compare the velocity profiles (normalised by the bulk velocity, U) for the four-mode Fluid 1 in Fig. 1(a) with those for the corresponding single-mode Fluid 2 in Fig. 1(b). Both PTT models have shear-thinning behaviour increasing with ε and the flow Deborah number, leading to blunter velocity profiles [7]. The Deborah number is calculated as $De = \lambda U/R$. The shear-thinning intensity of the corresponding single mode model is higher than that for the multi-mode model. For both fluids, and given the low value of ε, flows with $De \leq 0.1$ are basically Newtonian. These findings are also clear from the plots of normalized shear stress shown in Fig. 2. The stresses are normalized by the wall shear stress for a Newtonian fluid having the same total viscosity and flowing at the same flow rate, see Eq. (23), so that a Newtonian behavior is indicated by a linear variation from 0 on axis to 1 at the wall.

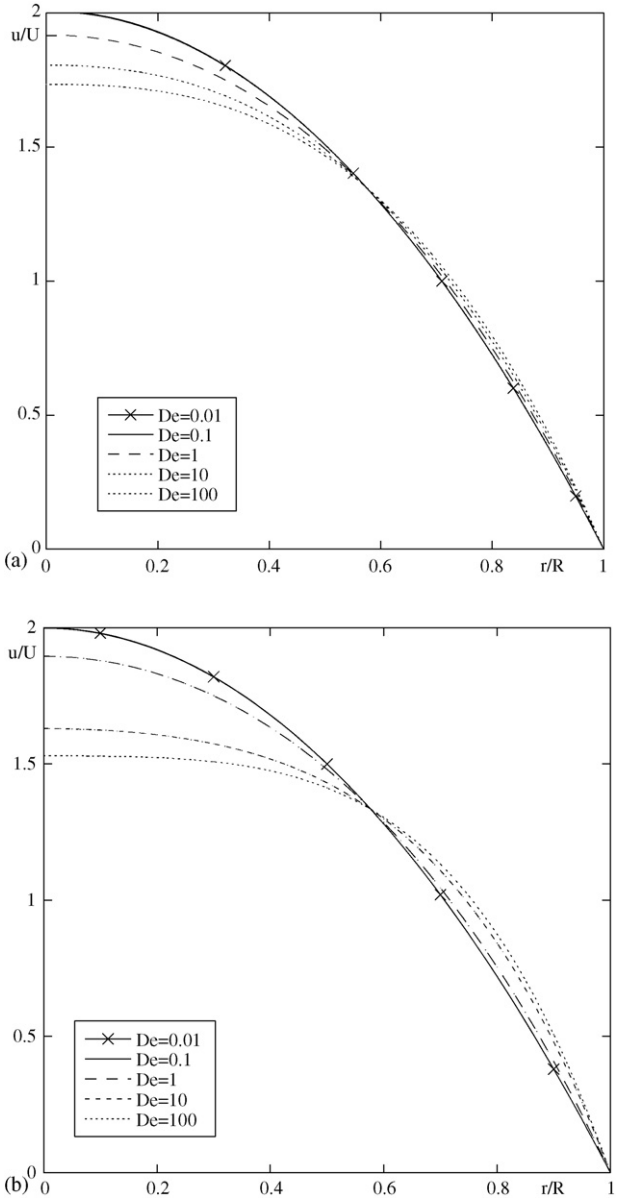

Fig. 1. Effect of Deborah number on the normalized velocity profiles for simplified PTT models with linear stress coefficient and $\varepsilon = 0.02$: (a) Fluid 1 (4 modes); (b) Fluid 2 (1 mode).

$$T_{rz} = \frac{\tau_{rz}}{4\eta(U/R)} \tag{23}$$

The stronger shear-thinning behaviour of Fluid 2 is clear from the lower values of T_{rz} in comparison with those of Fluid 1, under similar flow conditions.

The comparison between the elastic normal stresses $T_{zz,w}$ of the two fluids is shown in Fig. 3. The stresses are here normalized by the corresponding wall shear stress value of each fluid ($T_{zz,w} = \tau_{zz}/(\tau_{rz})_{\text{wall}}$) in order to remove the non-monotonic behaviour found by Oliveira and Pinho [7]. The multimode model is seen to be less elastic than the corresponding single mode model especially at high Deborah numbers (by a factor of 2.5 at $De = 100$), and the radial variation of $T_{zz,w}$ is also seen to

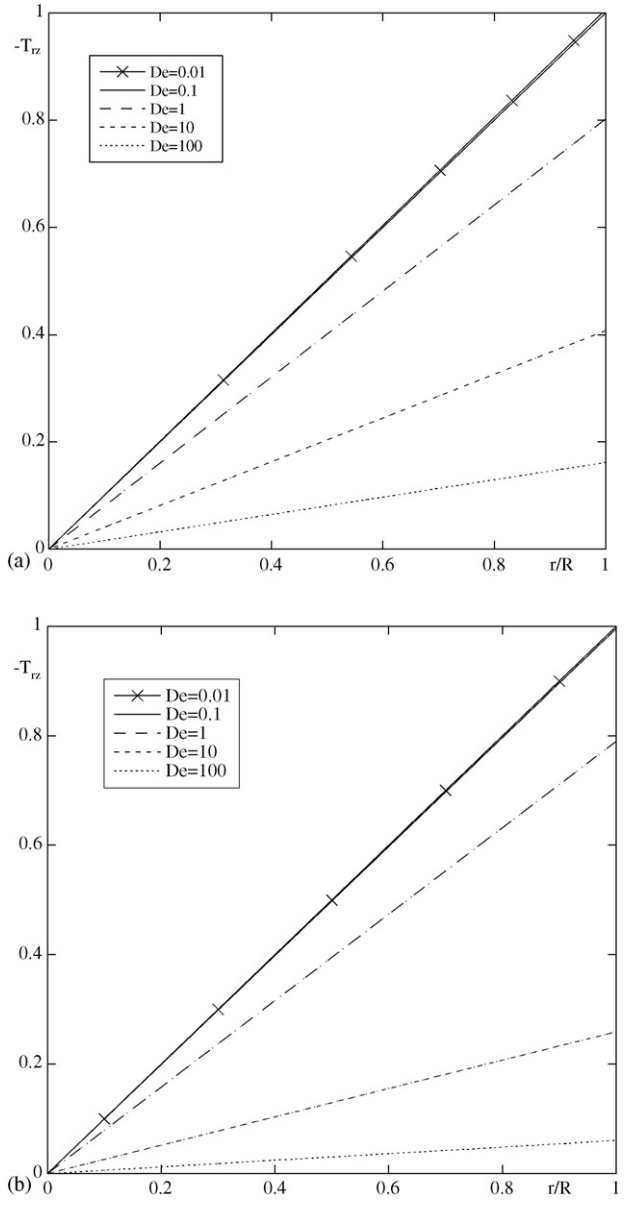

Fig. 2. Effect of Deborah number on the normalized profiles of extra shear stress (T_{rz}) for simplified PTT models with linear stress coefficient and $\varepsilon = 0.02$: (a) Fluid 1 (4 modes); (b) Fluid 2 (1 mode).

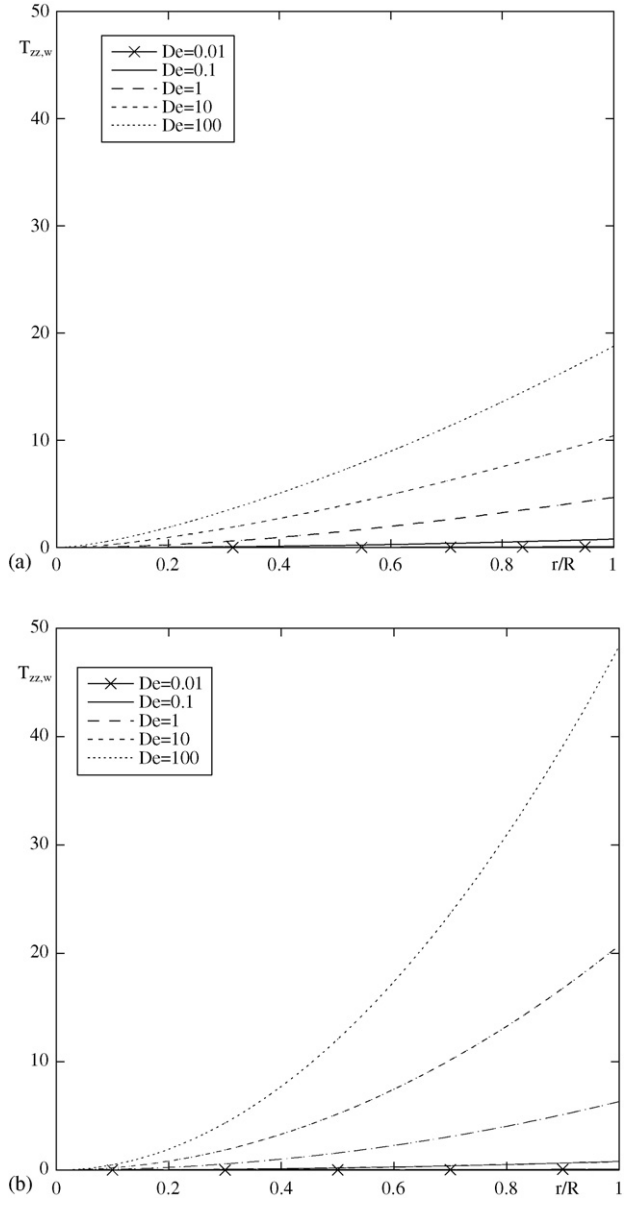

Fig. 3. Effect of Deborah number on the normalized profiles of extra normal stress (note the different normalization, $T_{zz,w}$) for simplified PTT models with linear stress coefficient with $\varepsilon = 0.02$: (a) Fluid 1 (4 modes); (b) Fluid 2 (1 mode).

be less non-linear for the multimode model than for the single mode model. This was expected, because the intensity of shear-thinning is directly proportional to the magnitude of the normal stress [7].

The similarity between Fluid 1 and the corresponding single mode model (Fluid 2) is exclusively based on the linear viscoelastic behaviour in the limit of low deformation rates (and low angular velocities). The two models behave differently in steady shear, as a quick comparison of the corresponding steady viscometric viscosity material functions would show. Next, we analyse in more detail the multimode solution, by looking at each individual mode and assessing its contribution to the total stress.

For Fluid 1, we plot in Fig. 4 the normal stress (left-half) and shear stress (right-half) for all modes, and the corresponding extra stress, at a low Deborah number of 0.01. All stresses were normalised according to Eq. (23). Since the velocity profile is basically Newtonian, the shear stresses of all modes vary linearly and their sum adds to 1 at the wall. The corresponding normal stresses are low, but non-zero, and they all vary quadratically as for Fluid 2 at very low Deborah numbers. Depending on the numerical values of the model parameters, it is already clear in Fig. 4 that different modes have different magnitudes for each stress component: in particular, lower modes tend to be more important for normal stresses than for shear stresses, whereas the opposite happens with the higher modes.

As the Deborah number increases and the velocity profile becomes shear-thinning, the individual modal shear stresses become nonlinear, the individual modal normal stresses are no

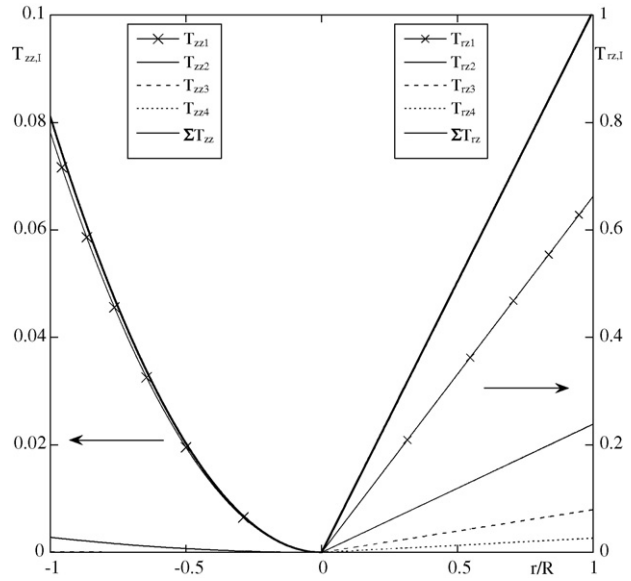

Fig. 4. Radial variation of the non-dimensional normal (T_{zz}) and shear (T_{rz}) stresses for all modes of Fluid 1 (linear PTT model, $\varepsilon = 0.02$, $\eta_s = 0$) at $De = 0.01$.

longer parabolic and the relative magnitudes between modes change, as is well shown in the stress plots of Fig. 5 for $De = 10$. The changes in the stresses for each mode are dramatic, exhibiting changes in the curvatures of the radial profiles so that profiles for different modes now cross each other (see modes 1 and 2 for the shear stress in Fig. 5). At higher Deborah numbers and/or values of ε, not shown here for compactness, these effects become even more pronounced. The normalised extra shear stress always varies linearly, but as shear thinning increases note that its wall value decreases from 1.

For the exponential PTT model, these features also take place.

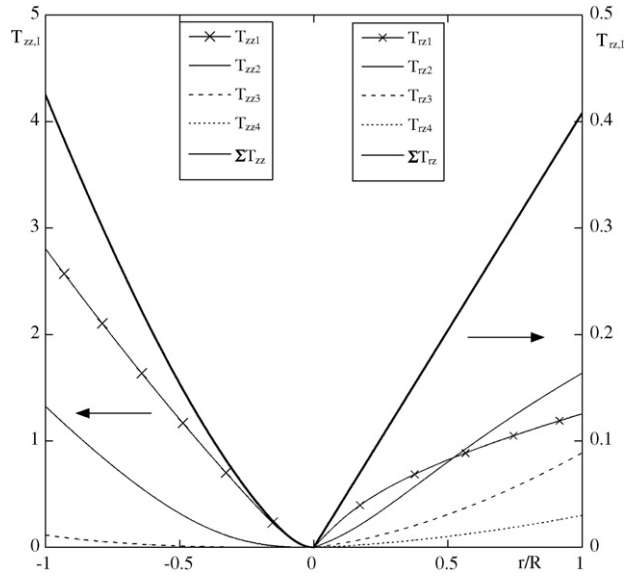

Fig. 5. Radial variation of the non-dimensional normal (T_{zz}) and shear (T_{rz}) stresses for all modes of Fluid 1 (linear PTT model, $\varepsilon = 0.02$, $\eta_s = 0$) at $De = 10$.

4. Approximate analytical solution

The method used here to obtain this solution for a multimode PTT model can, in principle, be used also for multimode models based on other single mode models. We start by defining

$$B_m \equiv \frac{\theta_m}{\theta_T} \quad \text{with} \quad \theta_m = \frac{\lambda_m \varepsilon_m}{\eta_m} \quad \text{and} \quad \theta_T = \sum_{m=1}^{N} \theta_m, \tag{24}$$

for the multimode PTT model (for a multimode Giesekus model the corresponding parameter would be $\theta_m \equiv \lambda_m \alpha_m / \eta_m$). When fitting multimode models to rheological data it is usual practice to consider the longest relaxation time as that of the first mode (cf. Table 1 and [5,18,19,24]) and as a consequence it is often the case that

$$B_1 > B_2 > \ldots > B_N. \tag{25}$$

In this approximate analysis this condition is enforced whenever it is not verified at the outset, by changing the order of the modes if necessary. Henceforth, we refer to the first mode as the principal mode (subscript p), and it is always the case that $B_m/B_p < 1$. Here, it is also assumed that

$$O\left(\frac{B_m}{B_p}\right)_{m \neq p} \ll 1 \tag{26}$$

which is often the case anyway. In Debbaut et al. [18], Debbaut and Dooley [19], Quinzani et al. [24] and Arigo and McKinley [25] for the worst cases $B_2/B_1 \approx 0.28$ and usually $B_2/B_1 \leq 0.15$.

Another quantity of interest in the present analysis is $\tilde{B}$, defined as

$$\tilde{B} \equiv \frac{\sum_{m=2}^{N} B_m}{N-1} \tag{27}$$

Given Eqs. (25) and (26), we can assume $O(\tilde{B}) \sim O(B_2)$ provided the number of modes is not too large (say, not exceeding 5, which is often the case in practical terms) even though $\tilde{B} < B_2$. Indeed, for a small number of modes we can even assume that $O(\tilde{B}) \sim O(B_m)$. This may no longer be true if the number of modes is large as in the work of Langouche and Debbaut [20], who used nine modes. In this case $O(\tilde{B}) \sim O(B_m)$ for $m \geq 3$ with the consequence that higher-order terms in $\tilde{B}$ may have to be retained (see next section).

4.1. Analytical solution

The solution of the governing equations can be written as an expansion on powers of $\tilde{B}$, where to a first approximation we neglect terms of order 2 and higher on account of the assumptions. Hence, the velocity u, the streamwise pressure gradient p_z and the ij stress component for each polymer mode ($\tau_{ij,m}$), except for the principal mode ($m = 1$), are given by

$$u = u_0 + \tilde{B} u_1 \tag{28a}$$

$$p_{,z} = p_{,z_0} + \tilde{B} p_{,z_1} \tag{28b}$$

$$\tau_{ij,m} = \tau_{ij,m_0} + B_m \tau_{ij,m_1} \quad \text{for } m = 2 \ldots N \tag{28c}$$

The main terms in Eq. (28), those on the right-hand-side with subscript 0, include effects from all stress modes as will be seen shortly. We also emphasize that Eq. (28c) is written in terms of B_m (rather than $\tilde{B}$) and that it decomposes the stress components of each mode, except for the principal mode (mode 1), which is dealt with exactly. If the constitutive equation includes a solvent its contribution to the total shear stress is also dealt with exactly (no decomposition). The total pressure gradient $p_{,z}$ can be decomposed in at least two ways: either as $p_{,z_0} = p_{,z}$ and $p_{,z_1} = 0$ or as $p_{,z_0} = p_{,z}(1 - \tilde{B})$ and $p_{,z_1} = p_{,z}$. The second set, or other choices that reduce the magnitude of $p_{,z_0}$, will result in less accuracy, therefore the first option is retained henceforth, i.e., $p_{,z_0} = p_{,z}$ and $p_{,z_1} = 0$.

Substituting Eq. (28) into the momentum equation, the following equations of zeroth and first order on $\tilde{B}$ ($\tilde{B}^0$ and $\tilde{B}^1$, respectively) are obtained after integration, and considering $O(\tilde{B}) \sim O(B_m)$ as explained above.

$$\tilde{B}^0 : p_{,z}\frac{r}{2} = \tau_{rz,1} + \eta_s\frac{du_0}{dr} + \sum_{m=2}^{N}\tau_{rz,m_0} \tag{29a}$$

$$\tilde{B}^1 : 0 = \eta_s\frac{du_1}{dr} + \sum_{m=2}^{N}\frac{B_m}{\tilde{B}}\tau_{rz,m_1} \tag{29b}$$

Since Eqs. (10) and (17) remain valid for any mode (subscript m instead of subscript p), substituting Eq. (28) into Eq. (17) for mode m, we arrive at Eqs. (30a) and (30b) by grouping terms of order $\tilde{B}^0$ and $\tilde{B}^1$, respectively.

$$\tilde{B}^0 : \eta_m\frac{du_0}{dr} = \tau_{rz,m_0} \tag{30a}$$

$$\begin{aligned}\tilde{B}^1 : \eta_m\frac{du_1}{dr} &= \frac{B_m}{\tilde{B}}\tau_{rz,m_1} + 2\frac{\lambda_m}{\eta_m}\frac{B_m}{\tilde{B}}\theta_T \\ &\times (\underline{\tau^3_{rz,m_0}} + 3B_m\tau^2_{rz,m_0}\tau_{rz,m_1} \\ &+ 3B^2_m\tau_{rz,m_0}\tau^2_{rz,m_1} + B^3_m\tau^3_{rz,m_1})\end{aligned} \tag{30b}$$

The last three terms inside the brackets on the right-hand-side of Eq. (30b) will be neglected, because they are of second and higher order on B_m. They will be important to assess the range of applicability of the approximate analytical solution discussed in Section 4.2.

Keeping only the underlined term inside the brackets, Eqs. (30a) and (30b) are inserted into the momentum Eqs. (29a) and (29b) yielding

$$p_{,z}\frac{r}{2} = \tau_{rz,1} + \left(\eta_s + \sum_{m=2}^{N}\eta_m\right)\frac{du_0}{dr} \tag{31a}$$

$$0 = \left(\eta_s + \sum_{m=2}^{N}\eta_m\right)\frac{du_1}{dr} - 2\sum_{m=2}^{N}\left(\frac{B_m\lambda_m\eta^2_m}{\tilde{B}}\right)\theta_T\left(\frac{du_0}{dr}\right)^3 \tag{31b}$$

These two differential equations must be solved to obtain the velocity profile. The solution of Eq. (31a) is similar to the solution for the pipe flow of a viscoelastic fluid represented by a one-mode PTT model plus Newtonian solvent derived by Cruz et al. [26], provided a new solvent viscosity coefficient, η_T, is made equal to $\left(\eta_s + \sum_{m=2}^{N}\eta_m\right)$. Hence, the solution of Eq. (31a) is

$$\begin{aligned}u_0(r) &= \frac{2U_{N,0}}{\beta_0}\left[1 - \left(\frac{r}{R}\right)^2\right] \\ &+ \frac{3}{8C\eta_T}\{F^+(R)G^-(R) - F^+(r)G^-(r) \\ &+ F^-(R)G^+(R) - F^-(r)G^+(r)\}\end{aligned} \tag{32}$$

where

$$\beta_0 \equiv \frac{\eta_T}{\eta_T + \eta_1} = \frac{\eta_s + \sum_{m=2}^{N}\eta_m}{\eta_s + \eta_1 + \sum_{m=2}^{N}\eta_m}; \quad U_{N,0} = \frac{-p_{,z}R^2}{8(\eta_T + \eta_1)};$$

$$C = \frac{\eta^2_1}{4\varepsilon_1\lambda^2_1}\frac{\eta_1}{\eta_T}\frac{p_{,z}}{2}; \quad A = \frac{\eta^2_1}{6\varepsilon_1\lambda^2_1}\left(1 + \frac{\eta_1}{\eta_T}\right) \tag{33}$$

$$F^{\pm}(r) = \left(Cr \pm \sqrt{A^3 + (Cr)^2}\right)^{1/3} \tag{34}$$

$$G^{\pm}(r) = 3Cr \pm \sqrt{A^3 + (Cr)^2} \tag{35}$$

Eq. (31b) is rearranged as

$$\frac{du_1}{dr} = \frac{2\theta_T}{\eta_T}\sum_{m=2}^{N}\left(\frac{B_m\lambda_m\eta^2_m}{\tilde{B}}\right)\left(\frac{du_0}{dr}\right)^3 \tag{36}$$

prior to integration and from Eq. (33) du_0/dr is calculated as

$$\frac{du_0}{dr} = \frac{p_{,z}}{2\eta_T}r - \frac{F^+(r)}{\eta_T} - \frac{F^-(r)}{\eta_T} \tag{37}$$

The solution of Eq. (36) is

$$\begin{aligned}u_1(r) &= \frac{\alpha CR^2}{4\eta^3_T}\left[1 - \left(\frac{r}{R}\right)^2\right] \\ &\times \left\{4 + 12AS - S^3C^2R^2\left[1 + \left(\frac{r}{R}\right)^2\right]\right\} \\ &+ \frac{9}{8}\frac{\alpha}{C\eta^3_T}A[F^+(r)G^-(r) + F^-(r)G^+(r) \\ &- F^+(R)G^-(R) - F^-(R)G^+(R)] \\ &+ \frac{9}{32}\frac{\alpha}{C\eta^3_T}S\{F^{+^2}(r)[3A^3 + 2CrG^-(r)] \\ &- F^{+^2}(R)[3A^3 + 2CRG^-(R)]\} \\ &+ \frac{9}{32}\frac{\alpha}{C\eta^3_T}S\{F^{-^2}(r)[3A^3 + 2CrG^+(r)] \\ &- F^{-^2}(R)[3A^3 + 2CRG^+(R)]\} + \frac{9}{320}\frac{\alpha}{C\eta^3_T}S^2 \\ &\times \sqrt{A^3 + (Cr)^2}[9A^3 - 4(Cr)^2][F^-(r) - F^+(r)]\end{aligned}$$

$$-\frac{9}{320}\frac{\alpha}{C\eta_T^3}S^2\sqrt{A^3+(CR)^2}[9A^3-4(CR)^2]$$
$$\times[F^-(R)-F^+(R)]+\frac{9}{320}\frac{\alpha}{C\eta_T^3}S^2 3Cr$$
$$\times[A^3-12(Cr)^2][F^-(r)+F^+(r)]$$
$$-\frac{9}{320}\frac{\alpha}{C\eta_T^3}S^2 3CR[A^3-12(CR)^2][F^-(R)+F^+(R)] \quad (38)$$

with $\alpha = 2\theta_T/(\eta_T\tilde{B}) \times \sum_{m=2}^{N}(B_m\lambda_m\eta_m^2)$ and $S = p_{,z}/2C$. For compactness, here it is also convenient to define $\Phi = \sqrt{A^3+(CR)^2}$.

The bulk velocity U is obtained from the integration of Eq. (28a)

$$U = \frac{1}{R^2}\left[\int_0^R 2ru_0(r)\mathrm{d}r + \tilde{B}\int_0^R 2ru_1(r)\mathrm{d}r\right] \quad (39)$$

and the result is presented as the following sum

$$U = \sum_{j=1}^{4}U_{0,j} + \tilde{B}\sum_{j=1}^{5}U_{1,j} \quad (40)$$

where the four $U_{0,j}$ terms and five $U_{1,j}$ terms are presented in Appendix A.

The extra shear and normal stresses follow from Eq. (2) and are calculated as

$$\tau_{rz} = \eta_s\dot{\gamma} + \tau_{rz,1} + \sum_{m=2}^{N}\tau_{rz,m} \quad (41)$$

$$\tau_{zz} = \tau_{zz,1} + \sum_{m=2}^{N}\tau_{zz,m} \quad (42)$$

The shear rate $\dot{\gamma}$ is defined as

$$\dot{\gamma} = \frac{\mathrm{d}u}{\mathrm{d}r} = \frac{\mathrm{d}u_0}{\mathrm{d}r} + \tilde{B}\frac{\mathrm{d}u_1}{\mathrm{d}r} \quad (43)$$

where the velocity derivatives are given by Eqs. (36) and (37).

The shear stress of the first mode comes from Eq. (17) using the relation of Eq. (10) between the shear and normal stresses. It is the solution of Eq. (17) and is given by

$$\tau_{rz,1} = \frac{\eta_1\dot{\gamma}}{1+\varepsilon_1\lambda_1/\eta_1 \times \tau_{zz,1}} \quad (44)$$

where the normal stress of the first mode ($\tau_{zz,1}$) is calculated using the solution of the cubic equation on this normal stress, derived by Alves et al. [8]. That solution is actually given by Eq. (14) with the coefficients of Eqs. (13) and (15), after setting $m=1$ and $\phi_p = 2\dot{\gamma}^2$.

For each of the higher modes, the shear stresses are given by

$$\tau_{rz,m} = \eta_m\dot{\gamma} - 2B_m\lambda_m\eta_m^2\theta_T\left(\frac{\mathrm{d}u_0}{\mathrm{d}r}\right)^3 \quad \text{for} \quad m = 2\ldots N \quad (45)$$

and the corresponding normal stresses are calculated using Eq. (10).

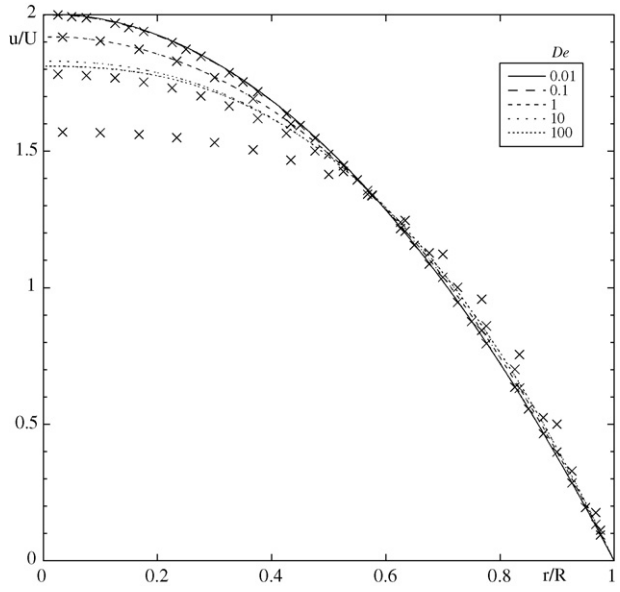

Fig. 6. Radial profiles of streamwise velocity for Fluid 1 (linear PTT model, $\varepsilon = 0.02$, $\eta_s = 0.27$ Pa s) as a function of Deborah number: comparison between the exact (lines) and approximate (symbols) solutions.

4.2. Results and discussion

We now compare this approximate analytical solution with the exact semi-analytical solution of Section 3 to assess the range of application of the former. The comparisons are carried out with Fluid 3, which is Fluid 1 with a Newtonian solvent contribution (see Table 1).

We plot in Fig. 6 radial profiles of streamwise velocity for Fluid 3 as a function of the Deborah number. Note that ε is constant and equal to 0.02. It is clear that the approximate solution approaches very well the exact semi-analytical solution for $De \leq 1$ (actually $\varepsilon De^2 \leq 0.02$), but shows stronger shear thinning for $De \geq 10$ (corresponding to $\varepsilon De^2 \geq 2$).

The corresponding plots of the shear and normal stresses are shown in Figs. 7 and 8 at $De = 1$ and 10, respectively. Note that the shear stress from the solvent is not plotted. For $De \leq 1$ the approximate solution reproduces the correct stresses for all modes. However, for $De = 10$ we observe that the total shear stress of the approximate solution is below that of the exact solution, an indication that the pressure gradient required to attain the same Deborah number is lower than in the approximate solution. For $De = 10$, we also see that the stresses of the first mode compare reasonably well with the corresponding exact stresses, but for the second mode ($T_{zz,2}$ and $T_{rz,2}$) the predictions by the approximate solution are clearly not good. In fact, the stresses of the first mode are dealt with exactly, but are also a consequence of the velocity profile, which was obtained with approximate stresses for the higher modes. Hence, the small differences between the first mode stresses of the exact and approximate solutions are a consequence of the differences in the velocity profile. However, the stresses of the second mode are approximated and when its shear component becomes relevant it is significantly different leading to the large differences observed in the velocity profile.

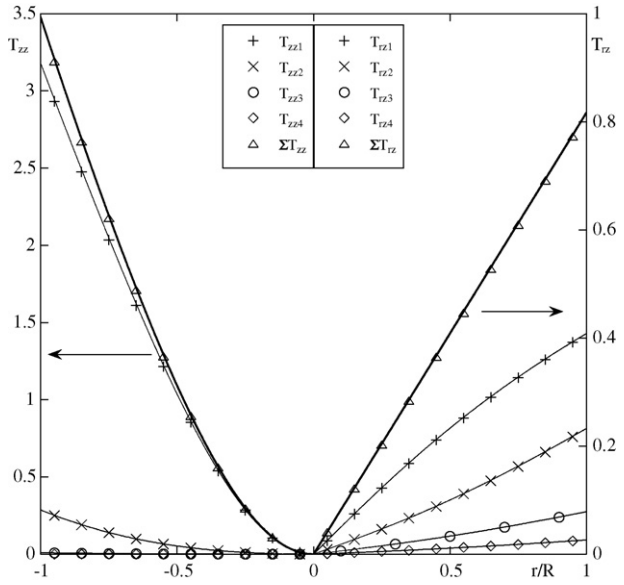

Fig. 7. Radial variation of the non-dimensional normal (T_{zz}) and shear (T_{rz}) stresses for the polymer modes of Fluid 3 (linear PTT model, $\varepsilon = 0.02$, $\eta_s = 0.27$ Pa s) at $De = 1$. Exact solution (lines); approximate solution (symbols).

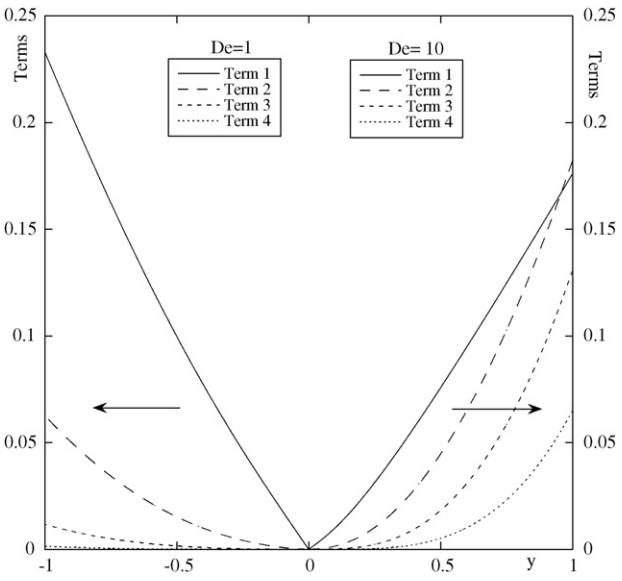

Fig. 9. Comparison between the terms within the brackets in Eq. (30b) for mode 2: Term 1 $= \tau_{rz,2_0}/(4\eta U/R)$, Term 2 $= (3B_2\tau_{rz,2_0}^2\tau_{rz,2_1})^{1/3}/(4\eta U/R)$, Term 3 $= (3B_2^2\tau_{rz,2_0}\tau_{rz,2_1}^2)^{1/3}/(4\eta U/R)$, Term 4 $= B_2\tau_{rz,2_1}/(4\eta U/R)$.

This raises the issue of the validity of the approximate solution and we look first at Eq. (30b) and in particular at the four terms inside the brackets. Using the approximate solution, these four terms were calculated for modes 2, 3 and 4 and for mode 2 they are compared in Fig. 9 for $De = 1$ and 10 in the form of normalized stresses. For $De = 1$ terms 2, 3 and 4 are indeed much smaller than term 1 that was kept in the analysis, and the more so because they enter Eq. (30b) as cubic powers of the plotted quantities. However, at $De = 10$ we clearly see that the first neglected term, term 2, has the magnitude of the non-neglected term near the wall (term 1), even though it is multiplied by B_2. For the third and fourth modes (not plotted) a similar situation arises, but because these stresses are smaller than $\tau_{rz,2}$ it looked as though they were well predicted in Fig. 8. As the Deborah number increases, the failure of the approximate solution is even clearer and the stresses for the higher modes (third and fourth order) will also be strongly affected.

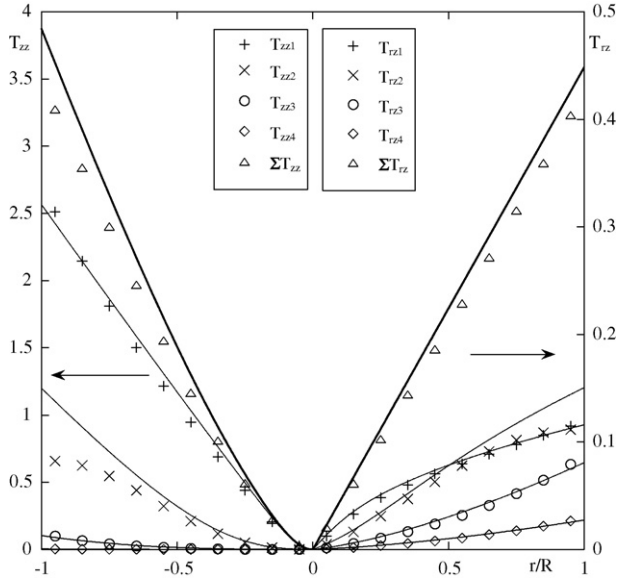

Fig. 8. Radial variation of the non-dimensional normal (T_{zz}) and shear (T_{rz}) stresses for the polymer modes of Fluid 3 (linear PTT model, $\varepsilon = 0.02$, $\eta_s = 0.27$ Pa s) at $De = 10$. Exact solution (lines); approximate solution (symbols).

The growth of the neglected terms is due to the growth of τ_{rz,m_1} which brings into question the assumptions of Eq. (28). The solution to the problem would be to consider higher order terms in the expansions of velocity and stress in Eqs. (28a) and (28c), leading to final expressions growing in complexity with progressively smaller gains in accuracy. Given this fact, and the availability of the exact solution of Section 3, we did not pursue the analytical solution further to higher order terms.

A criterion for validity of the approximate solution is presented below based on mode 2 and states that the second term within the brackets of Eq. (30b) must not exceed the underlined term, i.e.

$$\left|\frac{3B_2\tau_{rz,2_1}}{\tau_{rz,2_0}}\right| = \left|\frac{3\tilde{B}}{\tau_{rz,2_0}}\eta_2\frac{\mathrm{d}u_1}{\mathrm{d}r} - 6\frac{\lambda_2 B_2}{\eta_2}\theta_T\tau_{rz,2_0}^2\right| \ll 1 \tag{46}$$

Using Eqs. (30a) and (31b) to provide explicit expressions for $\tau_{rz,2_0}$ and $\mathrm{d}u_1/\mathrm{d}r$ we arrive at

$$\left|\frac{3B_2\tau_{rz,2_1}}{\tau_{rz,2_0}}\right| = 3\left(\frac{\mathrm{d}u_0}{\mathrm{d}r}\right)^2|\tilde{B}\alpha - 2\lambda_2 B_2\eta_2\theta_T| \tag{47}$$

This ratio is maximum at the wall and at the limiting condition we may consider, from Eq. (29a), that all its terms have the same

order of magnitude, hence we estimate

$$O\left(\left.\frac{\mathrm{d}u_0}{\mathrm{d}r}\right|_{\text{wall}}\right) = O\left(\frac{p_{,z}R}{2\eta_T}\right) \rightarrow \left.\frac{\mathrm{d}u_0}{\mathrm{d}r}\right|_{\text{wall}} \approx \frac{p_{,z}R}{2\eta_T} \tag{48}$$

Back-substituting, we arrive at

$$\left|\frac{3B_2\tau_{rz,2_1}}{\tau_{rz,2_0}}\right| = \frac{3}{4}\frac{p_{,z}^2R^2}{\eta_T^2}|\tilde{B}\alpha - 2\lambda_2 B_2\eta_2\theta_T| \ll 1 \tag{49}$$

providing the means to calculate the critical pressure gradient. Assuming that a ratio of 10% is sufficiently smaller than 1, the criterion for validity becomes

$$\left|\frac{3B_2\tau_{rz,2_1}}{\tau_{rz,2_0}}\right| = \frac{3}{4}\frac{p_{,z}^2R^2}{\eta_T^2}|\tilde{B}\alpha - 2\lambda_2 B_2\eta_2\theta_T| \approx \frac{1}{10} \tag{50}$$

Solving in order to $p_{,z}$ gives the maximum pressure gradient for which the approximate solution is an accurate multimode solution

$$p_{,z}|_{\max} = \frac{2\eta_T}{R}\sqrt{\frac{1}{3\times 10|\tilde{B}\alpha - 2\lambda_2 B_2\eta_2\theta_T|}} \tag{51a}$$

Due to the approximation invoked in Eq. (48), the exact value of $|3B_2\tau_{rz,2_1}/\tau_{rz,2_0}|$, for the imposed pressure gradient of Eq. (51a), was found to be around 30% rather than 10%, for various tested multimode models. At this condition the analytical solution is still a good approximation to the exact semi-analytical profiles as can be seen in Fig. 10 for Fluid 1 (by using a fluid without solvent contribution, we have a better test case since the solvent contribution is also dealt with without approximations).

The worst scenario is for identical values of B_m and in the absence of a solvent ($\eta_s = 0$), in which case all θ_m are also identical, $\theta_T = N\theta_m$ and $\tilde{B} = B_m = 1/N$. Since now $\eta_T = \sum_{m=2}^{N}\eta_m$ and considering $\eta_2^2\sum_{m=2}^{N}\eta_m \gg \sum_{m=2}^{N}\eta_m^3$, the criterion of validity of the approximation of Eq. (46), for the same 10% ratio, gives the following maximum pressure gradient

$$p_{,z}|_{\max} = \frac{\eta_T}{R\theta_2}\sqrt{\frac{2}{3\times 10\varepsilon_2}} \tag{51b}$$

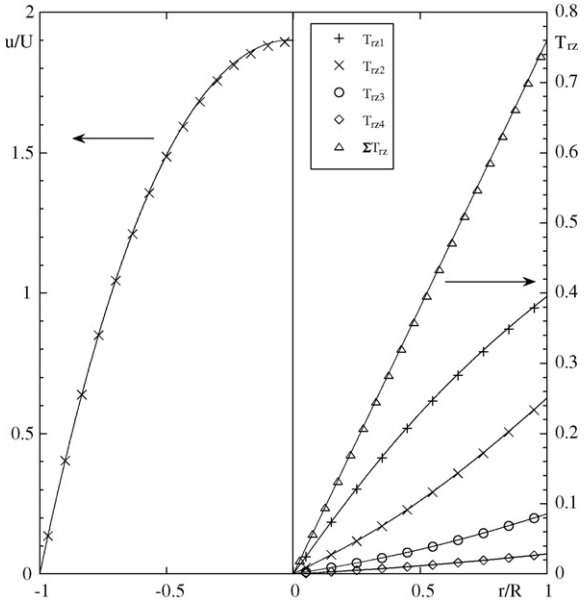

Fig. 10. Comparison between the radial profiles of normalized velocity and shear stresses for all modes of the exact and approximate solutions for the flow of fluid 1 at $De = 1.27$, corresponding to the limiting condition of Eq. (51a).

5. Other solutions

In this section, other solutions for multimode fluids are presented, without demonstration.

5.1. Approximate analytical solution for planar flow of linear PTT fluids

For the planar flow of half-height H the momentum equation (see Eq. (1)) is slightly different, but the process to obtain the solution remains the same. As for the pipe flow (Eq. (28a)), the velocity profile has two contributions

$$u(y) = u_0(y) + \tilde{B}u_1(y). \tag{52}$$

The first order velocity on the right-hand-side ($u_0(y)$) is exactly Eq. (32) except that the lateral coordinate is y, instead of r, and the half-width of the channel is H instead of R. The ratio of viscosities β_0 remains unchanged, but $U_{N,0}$ and C are defined differently as:

$$U_{N,0} = \frac{-p_{,z}H^2}{4(\eta_T+\eta_1)}; \quad C = \frac{\eta_1^2}{4\varepsilon_1\lambda_1^2}\frac{\eta_1}{\eta_T}p_{,z} \tag{53}$$

The second term on the right-hand-side of Eq. (52) ($u_1(y)$) is given by Eq. (38) the same equation as for pipe flow, provided r is substituted by y and R becomes H.

The bulk velocity is different from that of the pipe flow and is given by the following sum of thirteen terms, which are presented in Appendix B.

$$U = \frac{1}{H}\left[\int_0^H u_0(y)\mathrm{d}y + \tilde{B}\int_0^H u_1(y)\mathrm{d}y\right] \rightarrow U$$
$$= \sum_{j=1}^{4}U_{0,j} + \tilde{B}\sum_{j=1}^{9}U_{1,j} \tag{54}$$

The stress field for the planar flow is calculated as for pipe flow (Eqs. (41)–(45)) with the necessary adaptations in velocity profile and velocity derivatives.

5.2. Exact and approximate solutions for pipe and planar flows of multimode FENE-P fluids

The FENE-P model [27] can also be used in the context of a multimode constitutive equation, with the extra stress given as the sum of N polymer contributions and a Newtonian solvent, see Eq. (2). The contribution from each polymer mode obeys

the following expression

$$Z_m(\tau_{kk,m})\tau_{ij,m} + \lambda_m \overset{\nabla}{\tau}_{ij,m} - \lambda_m \left(\tau_{ij,m} + \frac{b_m}{b_m+2} n_m kT I_{ij}\right) \times \frac{D \ln Z_m(\tau_{kk,m})}{Dt} = 2\frac{b_m}{b_m+2} n_m kT \lambda_m D_{ij} \quad (55)$$

where $Z_m(\tau_{kk,m})$ is a function of the trace of the stress tensor. The various parameters of the model have specific physical meanings explained elsewhere [28], but the zero shear rate polymer viscosity coefficient for each mode is given by

$$\eta_m = n_m kT\lambda_m \frac{b_m}{b_m+5} \quad (56)$$

For fully-developed flow $D \ln Z/Dt = 0$ and Eq. (55) becomes similar to the constitutive equation for a PTT model [3]. A perfect match is obtained provided the following substitutions are made [26]:

$$\frac{b_m+2}{b_m+5} Z_m \to f_m; \quad \frac{b_m+2}{b_m+5}\lambda_m \to \lambda_m; \quad \frac{1}{b_m+5} \to \varepsilon_m; \quad \eta_m \to \eta_m \quad (57)$$

As a consequence, the solutions derived above for pipe and planar flows of the multimode PTT model apply equally to a multimode FENE-P fluid.

5.3. Exact solution for the Giesekus model

For the Giesekus model there is also a semi-analytical exact solution and in this section the equations that need to be solved are presented. The approach is identical to that described in Sections 2 and 3 for the PTT model, adapted to the Giesekus model and relying on the analytical solution for the one-mode Giesekus model of Schleiniger and Weinacht [4].

The momentum equation to be solved is again Eq. (1) and Eq. (2) also applies. The constitutive equation for a one-mode Giesekus model is given by expression (58)

$$\tau_{ij} + \lambda\left(\frac{\partial \tau_{ij}}{\partial t} + u_k\frac{\partial \tau_{ij}}{\partial x_k} - \tau_{jk}\frac{\partial u_i}{\partial x_k} - \tau_{ik}\frac{\partial u_j}{\partial x_k}\right) + \frac{\alpha\lambda}{\eta}\tau_{ik}\tau_{kj} = \eta\left(\frac{\partial u_i}{\partial x_j} + \frac{\partial u_j}{\partial x_i}\right) \quad (58)$$

introducing parameter α in the quadratic term, which is responsible for a non-zero second normal stress difference.

Adapting for each polymer mode, Schleiniger and Weinacht [4] gives the following expressions for the non-zero stresses in fully-developed Poiseuille flow:

$$\tau_{rz,m} = \eta_m\frac{du}{dr} + \lambda_m\tau_{rr,m}\frac{du}{dr} - \frac{\alpha_m\lambda_m}{\eta_m}(\tau_{zz,m} + \tau_{rr,m})\tau_{rz,m} \quad (59)$$

$$\tau_{zz,m} = 2\lambda_m\tau_{rz,m}\frac{du}{dr} - \frac{\alpha_m\lambda_m}{\eta_m}(\tau_{zz,m}^2 + \tau_{rz,m}^2) \quad (60)$$

$$\tau_{rr,m} = -\frac{\alpha_m\lambda_m}{\eta_m}(\tau_{rz,m}^2 + \tau_{rr,m}^2) \quad (61)$$

and with the solvent contribution still expressed by Eq. (8).

Following Schleiniger and Weinacht [4], the second order Eq. (61) gives for $\tau_{rr,m}$

$$\tau_{rr,m} = -\frac{\eta_m}{2\alpha_m\lambda_m} \pm \sqrt{\frac{\eta_m^2}{4\alpha_m^2\lambda_m^2} - \tau_{rz,m}^2} \quad (62)$$

and the shear rate is calculated by

$$\frac{du}{dr} = \frac{\tau_{rz,m}}{\eta_m}\frac{[1 + (2\alpha_m - 1)(\tau_{rr,m})/\eta_m]}{(1 + \lambda_m\tau_{rr,m}/\eta_m)^2}, \quad (63)$$

which depends on two stress components. Combining these two equations the velocity gradient is expressed as a function of the shear stress [4] for each mode as

$$\frac{du}{dr} = \frac{2\alpha_m\tau_{rz,m}}{\eta_m}\frac{[1 \pm (2\alpha_m - 1)\sqrt{1 - 4\alpha_m^2\lambda_m^2\tau_{rz,m}^2/\eta_m^2}]}{[\sqrt{1 - 4\alpha_m^2\lambda_m^2\tau_{rz,m}^2/\eta_m^2} \pm (2\alpha_m - 1)]^2} = \frac{2\alpha_p\tau_{rz,p}}{\eta_p}\frac{[1 \pm (2\alpha_p - 1)\sqrt{1 - 4\alpha_p^2\lambda_p^2\tau_{rz,p}^2/\eta_p^2}]}{[\sqrt{1 - 4\alpha_p^2\lambda_p^2\tau_{rz,p}^2/\eta_p^2} \pm (2\alpha_p - 1)]^2} \equiv \Phi_p \quad (64)$$

Since the right-hand-side of Eq. (64) is independent of the mode, it can be calculated using the principal mode which defines Φ_p.

Adapting Equation (3.3) of Schleiniger and Weinacht [4] $\tau_{zz,m}$ can now be calculated from Eq. (65) provided we know the other two stress components for the same mode. In this way, all quantities depend on $\tau_{rz,m}$.

$$\tau_{zz,m} = \eta_m\frac{du}{dr}\frac{1 + \lambda_m\tau_{rr,m}/\eta_m}{\alpha_m\lambda_m\tau_{rz,m}/\eta_m} - \frac{\eta_m}{\alpha_m\lambda_m}\left(1 + \frac{\alpha_m\lambda_m}{\eta_m}\tau_{rr,m}\right) \quad (65)$$

For the PTT model Eq. (10) was used to relate $\tau_{rz,m}$ with $\tau_{zz,m}$ and everything was equated in terms of $\tau_{zz,m}$ in order to benefit from the previous solution of Oliveira and Pinho [7]. For the Giesekus model, and using the second equality in Eq. (64), it is the shear stress $\tau_{rz,m}$ that is used assuming Φ_p is known.

$$\frac{2\alpha_m\tau_{rz,m}}{\eta_m}\left[1 \pm (2\alpha_m - 1)\sqrt{1 - \frac{4\alpha_m^2\lambda_m^2}{\eta_m^2}\tau_{rz,m}^2}\right] = \Phi_p\left[\sqrt{1 - \frac{4\alpha_m^2\lambda_m^2}{\eta_m^2}\tau_{rz,m}^2} \pm (2\alpha_m - 1)\right]^2 \quad (66)$$

Squaring Eq. (66) and making the substitution $T_m^2 = 1 - 4\alpha_m^2\lambda_m^2\tau_{rz,m}^2/\eta_m^2$ leads to a fourth order algebraic equation

$$\frac{1}{\lambda_m^2}(1-T_m^2)[1\pm(2\alpha_m-1)T_m]^2 = \Phi_p^2[T\pm(2\alpha_m-1)]^4 \quad (67)$$

for which algebra books provide a solution. Alternatively, it is also possible to obtain numerically values for $\tau_{rz,m}$, but we recommend the use of the algebraic solution in the spirit of the semi-analytical solution.

Once $\tau_{rz,m}$ is known as a function of the shear stress of the principal mode via Φ_p, the principal shear stress $\tau_{rz,p}$ is calculated solving the integrated momentum Eq. (68) (basically identical to that for the PTT; compare with Eq. (16) using Eq. (10)),

$$\frac{\mathrm{d}p}{\mathrm{d}z}\frac{r}{2^q} = \tau_{rz,p} + \sum_{m=2}^{N}\tau_{rz,m} + \eta_s\frac{\mathrm{d}u}{\mathrm{d}r} \quad (68)$$

where the velocity gradient is given by Eq. (69) and we also use $q=1$ for pipe flow and $q=0$ for planar flow.

$$\frac{\mathrm{d}u}{\mathrm{d}r} = \frac{2\alpha_p\tau_{rz,p}}{\eta_p}\frac{1\pm(2\alpha_p-1)\sqrt{1-4\alpha_p^2\lambda_p^2\tau_{rz,p}^2/\eta_p^2}}{\left[\sqrt{1-4\alpha_p^2\lambda_p^2\tau_{rz,p}^2/\eta_p^2}\pm(2\alpha_p-1)\right]^2} \quad (69)$$

Inserting Eq. (69) and the solution of Eq. (67) into Eq. (68), we have an analytical expression for the shear stress of the principal mode, $\tau_{rz,p}$. The velocity profile can now be obtained from numerical integration of Eq. (69).

6. Conclusions

Exact and approximate solutions are presented for fully-developed pipe and planar flows of multimode differential viscoelastic equations. The exact solutions are semi-analytic and pertain to models based on the Phan-Thien—Tanner (with $\xi=0$), Giesekus and FENE-P equations, whereas the approximate solutions are fully analytical and concern the PTT and FENE-P models. In all cases due account is taken of the presence of a Newtonian solvent.

The exact solutions show that at low Deborah numbers the flow is dominated by the low order stress modes, but the stresses from the higher modes increase and become of the same order as, and later exceed, those from the lower modes as the flow Deborah number progressively increases. These features are associated with the shear-thinning character of the models used and the relative values of the relaxation time and the flow characteristic time because the onset of shear-thinning takes place at a shear rate proportional to the reciprocal of the relaxation time. Therefore, as the flow Deborah number increases, the shear rates increase and the modes with higher relaxation times (lower modes) progressively contribute less to the shear stress balance, because of their decreasing shear viscosities, whereas those modes with a low relaxation time still contribute with viscosities close to their zero shear rate values.

The analytical approximate solution was obtained with a perturbation technique, but calculations with these formulae are limited to low values of flow Deborah number (actually to low values of εDe^2 for the PTT model and of the corresponding parameter for the FENE-P model, according to the transformation rules in Eq. (57). A criterion for the accurate use of this approximate solution is presented in Eqs. (50), (51a) and (51b). In spite of its length, the analytical solution is advantageous at low Deborah numbers because it eliminates the need for an iterative numerical procedure.

Fortran codes are available at http://www.fe.up.pt/~fpinho/research/menur.html to perform calculations with both the exact semi-analytical and approximate analytical solutions.

Acknowledgements

F.T. Pinho acknowledges funding from Fundação para a Ciência e Tecnologia and FEDER via research projects POCI56342/EQU/2004 and POCI59338/EME/2004.

Appendix A

The nine terms of Eq. (40) giving the bulk velocity of the approximate solution for pipe flow of the multimode PTT fluid

$$U_{0,1} = \frac{U_{N,0}}{\beta_0}$$

$$U_{0,2} = \frac{3}{8\eta_T C}\{F^+(R)G^-(R) + F^-(R)G^+(R)\}$$

$$U_{0,3} = \frac{9}{320R^2\eta_T C^3}\left\{F^+(R)\left[3\sqrt{A^3+(CR)^2}(A^3+4(CR)^2) - CR(A^3+28(CR)^2)\right] - 3A^5\right\}$$

$$U_{0,4} = \frac{-9}{320R^2\eta_T C^3}\left\{F^-(R)\left[3\sqrt{A^3+(CR)^2}(A^3+4(CR)^2) + CR(A^3+28(CR)^2)\right] + 3A^5\right\}$$

and, for compactness, using F^+ and F^- to represent the functions at the wall, i.e., $F^+(R)$ and $F^-(R)$,

$$U_{1,1} = \frac{-p_{,z1}R^2}{8\eta_T} + \frac{\alpha CR^2}{\eta_T^3}\left[\frac{1}{2} + \frac{3}{2}AS - \frac{S^3(CR)^2}{6} - \frac{9}{5}\frac{F^{-^2}}{A}\right] - \frac{81\alpha A^6}{160C^3\eta_T^3R^2}$$

$$U_{1,2} = \frac{-\alpha A^2}{960C^3\eta_T^3R^2(CR+\Phi)}\{81A^3[F^{+^2}(3\Phi+CR) + F^{-^2}(3\Phi+5CR)] + 108(CR)^2[2F^{-^2}(\Phi+5CR) - F^{+^2}(\Phi+9CR)]\}$$

$$\begin{aligned}U_{1,3} = {} & \frac{-9\alpha S}{2240C^3\eta_T^3R^4(CR+\Phi)^6}\{27A^{14}[3H(F^- - F^+) + CR(19F^- - 17F^+)] + 4A^{11}(CR)^2[-35F^+(9\Phi+17CR) \\ & + 44F^-(9\Phi+19CR)] + 112A^8(CR)^4[35F^-(\Phi+CR) - 4F^+(5\Phi+4CR)] - 64A^5(CR)^6[-28F^+(\Phi+2CR) \\ & + 5F^-(7\Phi+25CR)] - 256A^2(CR)^8[-14F^+(\Phi+CR) + 5F^-(11\Phi+15CR)] + 10240F^{+^2}(CR)^{10}\} - \frac{729\alpha A^7}{1120C^3\eta_T^3R^2}\end{aligned}$$

$$\begin{aligned}U_{1,4} = {} & \frac{-9\alpha S^2}{143360C^3\eta_T^3R^2(\Phi+CR)^4}\{3483A^{13}(F^{-^2}+F^{+^2}) + 774A^{10}CR[5F^{+^2}(3\Phi+5CR) + 7F^{-^2}(3\Phi+7CR)] \\ & + 16A^7(CR)^3[4F^{+^2}(222\Phi+199CR) + 7F^{-^2}(426\Phi+481CR)] + 32A^4(CR)^5[4F^{+^2}(-15\Phi+CR) \\ & + 7F^{-^2}(37\Phi+11CR)] + 256A(CR)^7[16F^{+^2}(\Phi+CR) + 7F^{-^2}(-4\Phi+CR)] + 17920(CR)^9F^+\} - \frac{31347\alpha A^8S^2}{71680C^3\eta_T^3R^2}\end{aligned}$$

$$\begin{aligned}U_{1,5} = {} & \frac{27\alpha S^2}{143360A^2C^3\eta_T^3R^2}\{[F^{-^2} - F^{+^2}]\Phi CR[342A^6 - 352A^3(CR)^2 + 3360(CR)^4] + [F^{-^2}+F^{+^2}][513A^9 + 114A^6(CR)^2 \\ & - 208A^3(CR)^4 + 3360(CR)^6]\} - \frac{13851A^8\alpha S^2}{71680C^3\eta_T^3R^2}\end{aligned}$$

Appendix B

The 13 terms of Eq. (54) giving the bulk velocity of the approximate solution for planar flow of the multimode PTT fluid

$$U_{0,1} = \frac{4U_{N,0}}{3\beta_0}$$

$$U_{0,2} = \frac{3}{8C\eta_T}[F^+(H)G^-(H) + F^-(H)G^+(H)]$$

$$U_{0,3} = \frac{9}{280H^2C^3\eta_T}\left\{F^+(H)\left[8A^3 + CH\left(-19CH + 9\sqrt{A^3+(CH)^2}\right)\right] - 8A^{7/2}\right\}$$

$$U_{0,4} = \frac{-9}{280H^2C^3\eta_T}\left\{F^-(H)\left[-8A^3 + CH\left(19CH - 9\sqrt{A^3+(CH)^2}\right)\right] + 8A^{7/2}\right\}$$

$$U_{1,1} = \frac{\alpha CH^2}{\eta_T^3}\left[\frac{2+6AS}{3} - \frac{C^2H^2S^3}{5}\right]$$

$$U_{1,2} = -\frac{9}{8}\frac{\alpha}{C\eta_T^3}A[F^+(H)G^-(H) + F^-(H)G^+(H)]$$

$$U_{1,3} = \frac{-9}{32}\frac{\alpha}{C\eta_T^3}S\{F^{+^2}(H)[3A^3 + 2CHG^-(H)] + F^{-^2}(H)[3A^3 + 2CHG^+(H)]\}$$

$$U_{1,4} = \frac{-9}{320}\frac{\alpha}{C\eta_T^3}S^2\sqrt{A^3+(CH)^2}[9A^3 - 4(CH)^2][F^-(H) - F^+(H)]$$

$$U_{1,5} = \frac{-9}{320}\frac{\alpha}{C\eta_T^3}S^2 3CH[A^3 - 12(CH)^2][F^-(H) + F^+(H)]$$

$$U_{1,6} = \frac{54 \times 44\alpha A}{77 \times 320HC^2\eta_T^3} F^-(H) \left\{ -8A^3 + 9CH\sqrt{A^3 + (CH)^2} + 19(CH)^2 \right\}$$
$$- \frac{216\alpha A}{7 \times 320H\eta_T^3} F^+(H) \left\{ 8A^3 + 9CH\sqrt{A^3 + (CH)^2} - 19(CH)^2 \right\}$$

$$U_{1,7} = \frac{54\alpha S}{320 \times 77C^2H\eta_T^3} \left\{ CH[641A^3 + 290(CH)^2][F^{+^2}(H) + F^{-^2}(H)] \right.$$
$$\left. + 6\sqrt{A^3 + (CH)^2}[64A^3 + 25(CH)^2][F^{-^2}(H) - F^{+^2}(H)] \right\}$$

$$U_{1,8} = \frac{81\alpha A^3 S^2}{35 \times 320C^2\eta_T^3 H} \left\{ 19CH\sqrt{A^3 + (CH)^2}[F^-(H) - F^+(H)] - 3[16A^3 - 3(CH)^2][F^-(H) + F^+(H)] \right\}$$

$$U_{1,9} = \frac{-108\alpha S^2}{5005 \times 320HC^2\eta_T^3} \left\{ 3CH\sqrt{A^3 + (CH)^2}[-92A^3 + 245(CH)^2][F^-(H) - F^+(H)] + CR[3815(CH)^4 \right.$$
$$\left. - 46A^3(CH)^2 - 828A^6][F^-(H) + F^+(H)] \right\}$$

References

[1] A.N. Beris, R.A. Armstrong, R.A. Brown, Perturbation theory for viscoelastic fluids between eccentric rotating cylinders, J. Non-Newt. Fluid Mech. 13 (1983) 109–143.

[2] D.O.A. Cruz, F.T. Pinho, Skewed Poiseuille-Couette flows of sPTT fluids in concentric annuli and channels, J. Non-Newt. Fluid Mech. 121 (2004) 1–14.

[3] P.J. Oliveira, An exact solution for tube and slit flow of a FENE-P fluid, Acta Mecanica 158 (2002) 157–167.

[4] G. Schleiniger, R.J. Weinacht, Steady Poiseuille flows for a Giesekus fluid, J. Non-Newt. Fluid Mech. 40 (1991) 79–102.

[5] J.Y. Yoo, HCh Choi, On the steady simple shear flows of the one-mode Giesekus fluid, Rheol. Acta 28 (1989) 13–24.

[6] J.J. Van Schaftingen, M.J. Crochet, Analytical and numerical solution of the Poiseuille flow of a Johnson–Segalman fluid, J. Non-Newt. Fluid Mech. 18 (1985) 335–351.

[7] P.J. Oliveira, F.T. Pinho, Analytical solution for fully-developed channel and pipe flow of Phan-Thien—Tanner fluids, J. Fluid Mech. 387 (1999) 271–280.

[8] M.A. Alves, F.T. Pinho, P.J. Oliveira, Study of steady pipe and channel flows of a single-mode Phan-Thien—Tanner fluid, J. Non-Newt. Fluid Mech. 101 (2001) 55–76.

[9] P.M. Coelho, F.T. Pinho, P.J. Oliveira, Thermal entry flow for a viscoelastic fluid: the Graetz problem for the PTT model, Int. J. Heat Mass Transfer 46 (2003) 3865–3880.

[10] S.H. Hashemabadi, S.G. Etemad, J. Thibault, M.R. Golkar-Naranji, Analytical solution for dynamic pressurization of viscoelastic fluids, Int. J. Heat Fluid Flow 24 (2003) 137–144.

[11] S.H. Hashemabadi, S.G. Etemad, M.R. Golkar-Naranji, J. Thibault, Mathematical modeling of laminar forced convection of simplified Phan-Thien—Tanner (SPTT) fluid between moving parallel plates, Int. Comm. Heat Mass Transfer 30 (2003) 197–205.

[12] M.A. Hulsen, Some properties and analytical expressions for plane flow of Leonov and Giesekus models, J. Non-Newt. Fluid Mech. 30 (1988) 85–92.

[13] M. Siline, A.I. Leonov, On flows of viscoelastic liquids in long channels and dies, Int. J. Eng. Sci. 39 (2001) 415–437.

[14] G.C. Georgiou, On the stability of shear flow of a viscoelastic fluid with slip along the fixed wall, Rheol. Acta 35 (1996) 39–47.

[15] G.C. Georgiou, D. Vlassopoulos, On the stability of the simple shear flow of a Johnson–Segalman fluid, J. Non-Newt. Fluid Mech. 75 (1998) 77–97.

[16] M.W. Johnson Jr., D. Segalman, A model for viscoelastic fluid behaviour which allows non-affine deformation, J. Non-Newt. Fluid Mech. 2 (1977) 255–270.

[17] M.M. Fyrillas, G.C. Georgiou, D. Vlasssopoulos, Time dependent plane Poiseuille flow of a Johnson–Segalman fluid, J. Non-Newt. Fluid Mech. 82 (1999) 105–123.

[18] B. Debbaut, T. Avalosse, J. Dooley, K. Hughes, On the development of secondary motions in straight channels induced by the second normal stress difference: experiments and simutations, J. Non-Newt. Fluid Mech. 69 (1997) 255–271.

[19] B. Debbaut, J. Dooley, Secondary motions in straight and tapered channels: experiments and three-dimensional finite element simulation with a multimode differential viscoelastic model, J. Rheol. 43 (1999) 1525–1545.

[20] F. Langouche, B. Debbaut, Rheological characterization of a high density polyethylene with a multimode differential viscoelastic model and numerical simulation of transient elongational recovery experiments, Rheol. Acta 38 (1999) 48–64.

[21] N. Phan-Thien, R.I. Tanner, A new constitutive equation derived from network theory, J. Non-Newt. Fluid Mech. 2 (1977) 353–365.

[22] M.A. Alves, D. Torres, M.P. Gonçalves, P.J. Oliveira, F.T. Pinho, Visualization of viscoelastic flows in a 4:1 3D contraction, in: AERC 2003 "Annual European Rheology Conference, Guimarães, Portugal, 11th–13th September, 2003, p. 2003.

[23] M.A. Alves, D. Torres, M.P. Gonçalves, P.J. Oliveira, F.T. Pinho, Visualization studies of viscoelastic flow in a 4:1 square/square contraction. Paper 1307, Flow Characterisation I, in CD-Rom, COBEM 2003 "17th International Congress of Mechanical Engineering", 10–14 November 2003, São Paulo, Brazil, 2003.

[24] L.M. Quinzani, G.H. McKinley, R.A. Brown, R.C. Armstrong, Modeling the rheology of polyisobutylene, J. Rheol. 34 (1990) 705–748.

[25] M.T. Arigo, G.H. McKinley, An experimental investigation of negative wakes behind spheres settling in a shear-thinning viscoelastic fluid, Rheol. Acta 37 (1998) 307–327.

[26] D.O.A. Cruz, F.T. Pinho, P.J. Oliveira, Analytical solution for fully-developed flow of some viscoelastic liquids with a Newtonian solvent contribution, J. Non-Newt. Fluid Mech. 132 (2005) 28–35.

[27] R.B. Bird, P.J. Dotson, N.L. Johnson, Polymer solution rheology based on a finitely extensible bead-spring chain model, J. Non-Newt. Fluid Mech. 7 (1980) 213–235.

[28] R.B. Bird, C.F. Curtiss, R.C. Armstrong, O. Hassager, Kinetic theory Dynamics of Polymeric Liquids, vol. 2, 2nd edition, John Wiley, New York, 1987.